



Naafs, B. D. A., Castro, J. M., de Gea, G. A., Quijano, M. L. L., Schmidt, D. N., & Pancost, R. D. (2016). Gradual and sustained carbon dioxide release during Aptian Oceanic Anoxic Event 1a. *Nature Geoscience*, 9(2), 135-139. <https://doi.org/10.1038/ngeo2627>

Peer reviewed version

Link to published version (if available):  
[10.1038/ngeo2627](https://doi.org/10.1038/ngeo2627)

[Link to publication record in Explore Bristol Research](#)  
PDF-document

## University of Bristol - Explore Bristol Research

### General rights

This document is made available in accordance with publisher policies. Please cite only the published version using the reference above. Full terms of use are available:  
<http://www.bristol.ac.uk/red/research-policy/pure/user-guides/ebr-terms/>

**Gradual and sustained carbon dioxide release during Aptian Oceanic Anoxic  
Event 1a**

B.D.A. Naafs<sup>1\*</sup>, J.M. Castro<sup>2</sup>, G.A. De Gea<sup>2</sup>, M.L. Quijano<sup>3</sup>, D.N. Schmidt<sup>4</sup>, and R.D.  
Pancost<sup>1</sup>

<sup>1</sup>Organic Geochemistry Unit, School of Chemistry and Cabot Institute, University of  
Bristol, BS8 1TS, UK

<sup>2</sup>Dept. Geología, CEACTION, University of Jaén, E-23071, Spain

<sup>3</sup>Dept. Química Inorgánica y Orgánica, CEACTION, University of Jaén, E-23071,  
Spain

<sup>4</sup>School of Earth Sciences and Cabot Institute, University of Bristol, BS8 1RJ, UK

\*Corresponding author. Tel. +44-(0)117-9546395. E-mail address:

[david.naafs@bristol.ac.uk](mailto:david.naafs@bristol.ac.uk)

**During the Aptian Oceanic Anoxic Event 1a, about 120 million years ago, black  
shales were deposited in all the major ocean basins<sup>1</sup>. The event was also  
associated with elevated sea surface temperatures<sup>2,3</sup> and a calcification crisis in  
calcareous nannoplankton<sup>4</sup>. These environmental changes have been attributed  
to variations in atmospheric CO<sub>2</sub> concentrations<sup>2,3,5,6</sup>, but the evolution of the  
carbon cycle during this event is poorly constrained. Here we present records of  
atmospheric CO<sub>2</sub> concentrations across Ocean Anoxic Event 1a derived from  
bulk and compound specific  $\delta^{13}\text{C}$  from marine rock outcrops in southern Spain  
and Tunisia. We find that CO<sub>2</sub> concentrations doubled in two steps during the**

ocean anoxic event and remained above background values for approximately 1.5 to 2 million years before declining. The rise of CO<sub>2</sub> concentrations occurred over several tens to hundreds of thousand years, and thus was unlikely to have resulted in any prolonged surface ocean acidification, suggesting that CO<sub>2</sub> emissions were not the primary cause of the nannoplankton calcification crisis. We find that the period of elevated CO<sub>2</sub> concentrations coincides with a shift in the oceanic osmium-isotope inventory<sup>7</sup> associated with emplacement of the Ontong Java Plateau flood basalts, and conclude that sustained volcanic outgassing was the primary source of carbon dioxide during Ocean Anoxic Event 1a.

Oceanic Anoxic Events (OAEs) represent dramatic changes in the climatic and palaeoceanographic state of the planet. Of these, OAE 1a during the Aptian Stage of the Early Cretaceous is one of the largest with black shale deposition in all major ocean basins<sup>1</sup>. Multi-proxy sea surface temperature (SST) estimates from the boreal realm and Pacific Ocean suggest that OAE 1a was accompanied by a ~ 4-8 °C increase in SSTs, assumed to be driven by an increase in  $p\text{CO}_2$ <sup>2,3</sup>. In addition, OAE 1a is concomitant with the calcification crisis of the nannoconids, the most ubiquitous planktic calcifiers during the Early Cretaceous<sup>4</sup>. Their near disappearance is one of the most significant events in the nannoplankton fossil record<sup>8</sup>. Their demise as well as malformation and secretion of dwarfed coccoliths and a reduction in pelagic carbonate fluxes have been suggested to represent a (calcification) response to widespread surface ocean acidification due to an increase in  $p\text{CO}_2$ <sup>5</sup>. However the source of excess CO<sub>2</sub>, potentially methane release from gas hydrates and/or CO<sub>2</sub> from (submarine) volcanic outgassing, the evolution of  $p\text{CO}_2$  across OAE 1a, and whether

51 this change in  $p\text{CO}_2$  is the driving factor for the calcification crisis remains  
52 controversial<sup>5-7,9-12</sup>. Most importantly, paleo- $p\text{CO}_2$  proxies have yet to confirm  
53 whether changes in  $p\text{CO}_2$  are indeed associated with these biological and  
54 environmental perturbations across OAE 1a and weather surface ocean acidification,  
55 defined here as a coupled decline in (surface) ocean pH and  $\Omega^{13}$  due to rapid input of  
56 carbon into the earth system, has happened at all. Determining the relative timing of  
57 events is crucial in identifying causal relationships and can provide crucial constraints  
58 for the source of  $p\text{CO}_2$ , but has been challenging as most records originate from slow  
59 accumulating deep-sea sediments.

60 To accurately determine the relative timing, we provide a high-resolution  
61 record of  $p\text{CO}_2$  across OAE 1a from an expanded section in Southern Spain (Cau, Fig.  
62 1). OAE 1a is defined as the interval covering segments C3-C6 and has a thickness of  
63  $\sim 40$  m at Cau, resulting in average sedimentation rate of 2.5 – 4 cm/ka, assuming an  
64 duration of 1-1.3 Myr<sup>14,15</sup>. These sedimentation rates are one order of magnitude  
65 higher than those at the OAE 1a reference section at Cismon, but similar to those at  
66 other expanded OAE 1a sections<sup>16,17</sup>. The hemipelagic sediments consisting of marls,  
67 marly limestones, and black marls (Fig. 2) that contain a rich and well-preserved  
68 fossil association, allowing for a detailed integrated bio- and chemostratigraphy<sup>18,19</sup>.  
69 Importantly, the organic matter at Cau is predominantly of marine origin and  
70 thermally immature<sup>20</sup>. The nannoconid crisis occurs around 42.5 m in the  
71 *Globigerinelloides blowi* planktonic foraminifera zone just before the beginning of the  
72 C3 segment and NCIE<sup>18,19</sup>, identical to other sections<sup>4,16</sup>.

73 To reconstruct changes in  $p\text{CO}_2$  we use paired bulk carbonate ( $\delta^{13}\text{C}_{\text{carb}}$ ) and  
74 organic carbon stable carbon isotopes (either bulk organic,  $\delta^{13}\text{C}_{\text{TOC}}$ , or based on algal  
75 derived lipids such as pristane,  $\delta^{13}\text{C}_{\text{alg}}$ ). The difference between these two records,



$\Delta^{13}\text{C}$  (for example,  $\Delta^{13}\text{C}_{\text{bulk}} = \delta^{13}\text{C}_{\text{carb}} - \delta^{13}\text{C}_{\text{TOC}}$ ), can be used to reconstruct changes in atmospheric  $\text{CO}_2$ <sup>21</sup> and has been applied to reconstruct changes in atmospheric  $p\text{CO}_2$  throughout Earth's history, including the OAEs<sup>22</sup>. The method relies on the understanding that high  $p\text{CO}_2$ , and hence dissolved  $\text{CO}_2$  concentrations in the surface ocean, cause greater discrimination against  $^{13}\text{C}$  during algal photosynthesis, leading to more depleted  $\delta^{13}\text{C}$  values for marine organic matter ( $\delta^{13}\text{C}_{\text{TOC}}$  and  $\delta^{13}\text{C}_{\text{alg}}$ ) compared to carbonates ( $\delta^{13}\text{C}_{\text{carb}}$ ). Here, we generate a high-resolution  $\Delta^{13}\text{C}_{\text{bulk}}$  record using  $\delta^{13}\text{C}_{\text{TOC}}$  determined for 114 samples through a 90-m sequence (Fig. 3a).

The  $\delta^{13}\text{C}_{\text{carb}}$  and  $\delta^{13}\text{C}_{\text{TOC}}$  profiles display all eight carbon isotope segments previously identified to be global<sup>23</sup> that are placed in a tight framework of biostratigraphy<sup>18,19</sup> with the characteristic negative and subsequent positive excursions related to the input of depleted carbon to the ocean-atmosphere and subsequent enhanced carbon burial under global greenhouse conditions (Fig. 2). The absolute values as well as the overall shape of the  $\delta^{13}\text{C}_{\text{carb}}$  curve, including the magnitude of the positive and negative excursion, are similar to those recorded around the globe (Fig. S1 and S2).

Biomarkers such as short-chain *n*-alkanes ( $\text{C}_{17}$  and  $\text{C}_{18}$ ) and pristane and phytane, the latter two derived from phytanyl side chains of the chlorophylls of algae and cyanobacteria, can serve as proxies for the isotopic composition of phytoplankton<sup>10,24</sup>. A lower-resolution record of compound-specific  $\delta^{13}\text{C}$  from Cau was generated using these biomarkers (Fig. 2b), which in our samples predominantly derive from algae ( $\delta^{13}\text{C}_{\text{alg}}$ ).  $\delta^{13}\text{C}_{\text{alg}}$  was determined for a total of 19 samples and range from -24 to -34.5 ‰ (or -20 to -30.5 ‰ when corrected to bulk biomass), with the lowest values during the later stage of isotope segments C3 and C4 (Fig. 2b). The shapes as well as absolute values of  $\delta^{13}\text{C}_{\text{alg}}$  are very similar to  $\delta^{13}\text{C}_{\text{TOC}}$ , indicating that

$\delta^{13}\text{C}_{\text{TOC}}$  is not significantly influenced by changes in the composition of bulk organic matter via either changes in source input or diagenesis. This suggests that the majority of organic matter at Cau is of marine (algal) origin, which is consistent with the overall biomarker assemblage<sup>20</sup>.

The  $\delta^{13}\text{C}_{\text{alg}}$  values are also similar to those reported from other (low-resolution) records across OAE 1a. Taken together this demonstrates that the  $\delta^{13}\text{C}_{\text{alg}}$  we report from Cau are typical for OAE 1a. The similarity of  $\delta^{13}\text{C}_{\text{alg}}$  compared to other OAE 1a records together with the absence of major changes in total organic carbon content (Fig. S4) and biomarker distribution across OAE 1a suggest that changes in algal composition (Fig. S3), physiology, or nutrient contents of the waters are unlikely to have had a significantly effect, mitigating concerns associated with growth rate impacts on  $\delta^{13}\text{C}$  records. The negative shift in  $\delta^{13}\text{C}_{\text{TOC}}$  values, similar to that seen in  $\delta^{13}\text{C}_{\text{alg}}$ , and resulting positive excursion in the  $\Delta^{13}\text{C}_{\text{bulk}}$  record between 55 and 90 m therefore predominantly indicates a greater discrimination against  $^{13}\text{C}$  during algal photosynthesis due to elevated  $p\text{CO}_2$  levels (Fig. 3a).

Using  $\delta^{13}\text{C}_{\text{alg}}$  we then tentatively quantified  $p\text{CO}_2$  by converting  $\Delta^{13}\text{C}$  values into  $\epsilon_p$  (carbon isotope discrimination during photosynthesis) and using modern relationships between  $\epsilon_p$  and  $\{\text{CO}_2(\text{aq})\}$ . The absolute  $\text{CO}_2$  values are calculated using a number of assumptions for palaeoproductivity, sea surface temperature, and equilibrium  $\text{CO}_2$  exchange between ocean and atmosphere and should be considered as estimates. Pre-OAE 1a values are estimated between 800 and 1200 ppmv (Fig. 3b), entirely consistent with low-resolution multi-proxy estimates of (Early) Cretaceous background  $p\text{CO}_2$ <sup>13,25</sup>. During OAE 1a, specifically the latter part of segment C3-C4,  $p\text{CO}_2$  doubled to values between 1400 and 2800 ppmv. We support the minimum  $p\text{CO}_2$  values during segment C3 and maximum  $p\text{CO}_2$  values during segment C4 by

providing low-resolution independent  $p\text{CO}_2$  estimates from the Djebel Serdj section from Tunisia<sup>26</sup> (Fig. 3b). The values, which were obtained using compound-specific  $\delta^{13}\text{C}_{\text{alg}}$  and the exact same assumptions as used to calculate  $p\text{CO}_2$  at Cau, range between 1100 and 2000 ppmv with the highest values during C4. The similarity in absolute  $p\text{CO}_2$  values between the two records demonstrates that the high-resolution  $p\text{CO}_2$  record from Cau represents a global signal and is not significantly biased by local factors. It is important to note that due to the non-linear nature of the  $\varepsilon_p$  and  $\{\text{CO}_2(\text{aq})\}$ -relationship the higher  $p\text{CO}_2$  values could be underestimates.

The  $p\text{CO}_2$  record for the first time depicts the often-inferred increase and decrease in  $p\text{CO}_2$  across segments later part of C3 to mid-C7 (Fig. 3a-b). As segments C3-C6 (OAE 1a) are estimated to represent around 1.1 Myrs and segment C7 an additional 1.6 Myrs<sup>15</sup>, the period of elevated “super greenhouse”  $\text{CO}_2$  levels, likely lasted around 1.5 to 2 Myrs. The continuously high  $p\text{CO}_2$  values during segments C4-C6 suggest constant input of carbon into the ocean-atmosphere system, almost balanced by extensive organic matter burial in black shales around the world as indicated by the positive  $\delta^{13}\text{C}_{\text{carb}}$  excursion.

The timing of the  $p\text{CO}_2$  increase that starts in the middle of segment C3 provides critical constraints on the source of excess  $\text{CO}_2$  during OAE 1a. Records from the Pacific and Tethys realms demonstrate that during OAE 1a the global oceanic Osmium (Os) isotope composition was exceptionally unradiogenic (mantle-like), interpreted to reflect the main phase of eruption of the Ontong Java plateau<sup>7,27</sup>. The major shift in Os-isotopes and hence eruption phase occurs well after the onset of the nannoconid crisis during the middle of segment C3, at the same time as the onset of  $\Delta^{13}\text{C}_{\text{bulk}}/p\text{CO}_2$  increase at Cau (Fig. 3c). The simultaneous shifts in Os-isotopes and

$p\text{CO}_2$  provides compelling evidence that the source of excess  $\text{CO}_2$  is derived from volcanic outgassing related to the emplacement of the Ontong Java Plateau.

In addition, the initial two-step rise in  $\Delta^{13}\text{C}_{\text{bulk}}/p\text{CO}_2$  during segment C3-C4 spans roughly 10 meters in our section from 55 to 65 m (Fig. 3). Estimates from other expanded sections suggest a duration of 100-300 kyr for C3<sup>16,17</sup>, resulting in average sedimentation rates of 5 to 15 cm/kyr for this segment. Combined with the assumed duration of segment C4 of 200-280 kyr<sup>15</sup>, the  $\text{CO}_2$  doubling took at least 100 kyr and very likely more than 300 kyr.

Previous studies argued that the nanoconid crisis was caused by widespread and sustained surface ocean acidification due to numerous pulses of  $\text{CO}_2$  and methane, with the first pulse coinciding with the onset of the nannoconid crisis during carbon isotope segment C2<sup>5</sup>. However, our high-resolution  $p\text{CO}_2$  record challenges this. Our record indicates a gradual and sustained, two-step increase in  $p\text{CO}_2$ , likely volcanic sourced, during the latter part of segment C3 and C4 that took place over at least 100 kyr and occurred well after the onset of the nannoconid crisis. Such a slow ( $> 10$  kyr)  $\text{CO}_2$  release is buffered in the ocean by dissolution of carbonates in deep-sea sediments combined with silicate rock weathering on land and, assuming no major spatial shift in carbonate burial, would have prevented a coupled decline in pH and  $\Omega^{28,29}$ . Due to current uncertainties in determining absolute ages or durations in the Early Cretaceous we cannot completely rule-out very brief episodes of surface ocean acidification during the latter part of segment C3 and C4 when  $p\text{CO}_2$  increases. However, the significant lag ( $\sim 10$  m, representing at least 60 kyr during C3) between the onset of the nannoconid crisis and onset of  $\text{CO}_2$  increase and shift in Os-isotopes (Fig. 3) clearly demonstrates that  $\text{CO}_2$ -induced surface ocean acidification could not have caused the nannoconid crisis.

In summary, our records demonstrate that OAE 1a was associated with a gradual, two-step increase in  $p\text{CO}_2$  to values roughly double that of pre-OAE 1a values. The similarity in timing between changes in  $p\text{CO}_2$  and oceanic Os-isotope inventory suggests that volcanic outgassing associated with the emplacement of the Ontong Java Plateau was the dominant source of  $\text{CO}_2$ . The prolonged duration of  $p\text{CO}_2$  increase, and by extension the total amount of released carbon, indicates that methane release from gas hydrates was not likely a major source of  $p\text{CO}_2$  during OAE 1a.

## References

- 1 Jenkyns, H. C. Geochemistry of oceanic anoxic events. *Geochem. Geophys. Geosy.* **11**, Q03004 (2010).
- 2 Mutterlose, J., Bottini, C., Schouten, S. & Sinninghe Damsté, J. S. High sea-surface temperatures during the early Aptian Oceanic Anoxic Event 1a in the Boreal Realm. *Geology* **42**, 439-442 (2014).
- 3 Ando, A., Kaiho, K., Kawahata, H. & Kakegawa, T. Timing and magnitude of early Aptian extreme warming: Unraveling primary  $\delta^{18}\text{O}$  variation in indurated pelagic carbonates at Deep Sea Drilling Project Site 463, central Pacific Ocean. *Palaeogeogr., Palaeoclimatol., Palaeoecol.* **260**, 463-476 (2008).
- 4 Erba, E. Nannofossils and Superplumes: The Early Aptian "Nannoconid Crisis". *Paleoceanography* **9**, 483-501 (1994).
- 5 Erba, E., Bottini, C., Weissert, H. J. & Keller, C. E. Calcareous Nannoplankton Response to Surface-Water Acidification Around Oceanic Anoxic Event 1a. *Science* **329**, 428-432 (2010).
- 6 Méhay, S. *et al.* A volcanic  $\text{CO}_2$  pulse triggered the Cretaceous Oceanic Anoxic Event 1a and a biocalcification crisis. *Geology* **37**, 819-822 (2009).
- 7 Bottini, C., Cohen, A. S., Erba, E., Jenkyns, H. C. & Coe, A. L. Osmium-isotope evidence for volcanism, weathering, and ocean mixing during the early Aptian OAE 1a. *Geology* **40**, 583-586 (2012).
- 8 Kump, L. R., Bralower, T. J. & Ridgwell, A. Ocean acidification in deep time. *Oceanography* **22**, 94-107 (2009).
- 9 Gibbs, S. J., Robinson, S. A., Bown, P. R., Jones, T. D. & Henderiks, J. Comment on "Calcareous Nannoplankton Response to Surface-Water Acidification Around Oceanic Anoxic Event 1a". *Science* **332**, 175 (2011).
- 10 Heimhofer, U., Hochuli, P. A., Herrle, J. O., Andersen, N. & Weissert, H. Absence of major vegetation and palaeoatmospheric  $p\text{CO}_2$  changes associated with oceanic anoxic event 1a (Early Aptian, SE France). *Earth Plant. Sc. Lett.* **223**, 303-318 (2004).
- 11 van Breugel, Y. *et al.* Synchronous negative carbon isotope shifts in marine and terrestrial biomarkers at the onset of the early Aptian oceanic anoxic event

1a: Evidence for the release of  $^{13}\text{C}$ -depleted carbon into the atmosphere. *Paleoceanography* **22**, PA1210 (2007).

12 Beerling, D. J., Lomas, M. R. & Gröcke, D. R. On the nature of methane gas-hydrate dissociation during the Toarcian and Aptian Oceanic anoxic events. *Am. J. Sci.* **302**, 28-49 (2002).

13 Hönisch, B. *et al.* The Geological Record of Ocean Acidification. *Science* **335**, 1058-1063 (2012).

14 Li, Y.-X. *et al.* Toward an orbital chronology for the early Aptian Oceanic Anoxic Event (OAE1a, ~ 120 Ma). *Earth Plant. Sc. Lett.* **271**, 88-100 (2008).

15 Malinverno, A., Erba, E. & Herbert, T. D. Orbital tuning as an inverse problem: Chronology of the early Aptian oceanic anoxic event 1a (Selli Level) in the Cismon APTICORE. *Paleoceanography* **25**, PA2203 (2010).

16 Kuhnt, W., Holbourn, A. & Moullade, M. Transient global cooling at the onset of early Aptian oceanic anoxic event (OAE) 1a. *Geology* **39**, 323-326 (2011).

17 Lorenzen, J. *et al.* A new sediment core from the Bedoulian (Lower Aptian) stratotype at Roquefort-La Bédoule, SE France. *Cretaceous Res.* **39**, 6-16 (2013).

18 de Gea, G. A., Castro, J. M., Aguado, R., Ruiz-Ortiz, P. A. & Company, M. Lower Aptian carbon isotope stratigraphy from a distal carbonate shelf setting: the Cau section, Prebetic zone, SE Spain. *Palaeogeogr., Palaeoclimatol., Palaeoecol.* **200**, 207-219 (2003).

19 Aguado, R., Castro, J. M., Company, M. & Alfonso De Gea, G. Aptian bio-events—an integrated biostratigraphic analysis of the Almadich Formation, Inner Prebetic Domain, SE Spain. *Cretaceous Res.* **20**, 663-683 (1999).

20 Quijano, M. L. *et al.* Organic geochemistry, stable isotopes, and facies analysis of the Early Aptian OAE-New records from Spain (Western Tethys). *Palaeogeogr., Palaeoclimatol., Palaeoecol.* **365-366**, 276-293 (2012).

21 Kump, L. R. & Arthur, M. A. Interpreting carbon-isotope excursions: carbonates and organic matter. *Chem. Geol.* **161**, 181-198 (1999).

22 Jarvis, I., Lignum, J. S., Gröcke, D. R., Jenkyns, H. C. & Pearce, M. A. Black shale deposition, atmospheric  $\text{CO}_2$  drawdown, and cooling during the Cenomanian-Turonian Oceanic Anoxic Event. *Paleoceanography* **26**, PA3201 (2011).

23 Menegatti, A. P. *et al.* High-Resolution  $\delta^{13}\text{C}$  Stratigraphy Through the Early Aptian "Livello Selli" of the Alpine Tethys. *Paleoceanography* **13**, 530-545 (1998).

24 Sinninghe Damsté, J. S., Kuypers, M. M. M., Pancost, R. D. & Schouten, S. The carbon isotopic response of algae, (cyano)bacteria, archaea and higher plants to the late Cenomanian perturbation of the global carbon cycle: Insights from biomarkers in black shales from the Cape Verde Basin (DSDP Site 367). *Org. Geochem.* **39**, 1703-1718 (2008).

25 Royer, D. L., Pagani, M. & Beerling, D. J. Geobiological constraints on Earth system sensitivity to  $\text{CO}_2$  during the Cretaceous and Cenozoic. *Geobiology* **10**, 298-310 (2012).

26 Heldt, M., Bachmann, M. & Lehmann, J. Microfacies, biostratigraphy, and geochemistry of the hemipelagic Barremian–Aptian in north-central Tunisia: Influence of the OAE 1a on the southern Tethys margin. *Palaeogeogr., Palaeoclimatol., Palaeoecol.* **261**, 246-260 (2008).

27 Tejada, M. L. G. *et al.* Ontong Java Plateau eruption as a trigger for the early Aptian oceanic anoxic event. *Geology* **37**, 855-858 (2009).

- 28 Ridgwell, A. & Schmidt, D. N. Past constraints on the vulnerability of marine calcifiers to massive carbon dioxide release. *Nature Geosci.* **3**, 196-200 (2010).
- 29 Uchikawa, J. & Zeebe, R. E. Examining possible effects of seawater pH decline on foraminiferal stable isotopes during the Paleocene-Eocene Thermal Maximum. *Paleoceanography* **25**, PA2216 (2010).

## Acknowledgements

BDAN received funding through a Rubicon fellowship, awarded by the Netherlands Organisation for Scientific Research (NWO). Additional funding came from the advanced ERC grant “The greenhouse earth system” (T-GRES). JMC and MLQ were funded by University of Jaén fellowships, DNS was funded by a Royal Society URF. RDP and DNS acknowledge the Royal Society Wolfson Research Merit Award. We wish to thank the University of Jaén (CICT) for the use of analytical facilities and NERC for partial funding of the mass spectrometry facilities at the University of Bristol (contract no. R8/H10/63; [www.lsmsf.co.uk](http://www.lsmsf.co.uk)). Matthias Heldt is thanked for providing the samples from Djebel Serdj. This work is a contribution of the research project CGL2009-10329 and CGL2014-55274-P (Spanish Ministry of Science and Technology), “Episodios de Cambio Climático Global” (Instituto de Estudios Giennenses) and RNM-200 (Junta de Andalucía).

## Author contributions

BDAN, DNS, and RDP designed the study. JMC and GAD generated the stratigraphy, gathered the samples in the field, and prepared the samples for bulk stable isotope analyses. MLQ and JMC conducted the biomarker extraction and characterization of samples from Cau. BDAN performed the biomarker extraction of samples from Djebel Serdj, measured all compound specific isotope data for Cau and Djebel Serdj, and wrote the manuscript with contribution from all authors.

## Competing financial interested

We declare no competing financial interests.

## Figure Legends

### Figure 1; Study area

Palaeogeographic reconstruction of the Tethys region during the Aptian. The approximated locations of Cau and Djebel Serdj, as well as other key-OAE 1a

sections are indicated by red and black stars, respectively. Figure modified from R. Blakey, <http://cpgeosystems.com/euromaps.html>.

**Figure 2; Carbon isotope records from Cau across OAE 1a**

a) bulk carbonate stable carbon isotopes (light blue circles) and b) total organic matter stable carbon isotopes (dark blue circles) together with compound specific stable carbon isotopes of pristane (green circles), phytane (red diamonds), C<sub>17</sub> (orange triangles) and C<sub>18</sub> *n*-alkanes (brown reversed triangles). Error bars on compound specific stable carbon isotope data reflect 1σ of replicates. Isotope segments according to Menegatti et al.<sup>23</sup>. δ<sup>13</sup>C<sub>alg</sub> is corrected to bulk biomass by adding 4 ‰.

**Figure 3; Estimates of atmospheric CO<sub>2</sub> across OAE 1a**

a) High-resolution of Δ<sup>13</sup>C<sub>bulk</sub> at Cau together with b) *p*CO<sub>2</sub> estimate based on δ<sup>13</sup>C<sub>alg</sub> from Cau (orange diamonds) and Djebel Serdj (purple circles), and c) <sup>187</sup>Os/<sup>188</sup>Os record from Cismon<sup>7</sup>. The duration of the nannoconid crisis at Cau<sup>19</sup> and Cismon<sup>5</sup> is indicated by green bars. Turquoise shading in a) represent uncertainty in Δ<sup>13</sup>C<sub>bulk</sub>, orange shading in b) represents the uncertainty in *p*CO<sub>2</sub>-estimates related to uncertainty in δ<sup>13</sup>C<sub>carb</sub> and growth rate and cell geometry (the *b*-value), while light-yellow shading is the superimposed spread in the different δ<sup>13</sup>C<sub>alg</sub> for a specific sample.



## Material and methods

### Data collection

The Cau section was completed re-logged and remeasured. Bulk C-isotope analyses of the carbonate fraction ( $\delta^{13}\text{C}_{\text{carb}}$ ) were carried out at the Stable Isotope Laboratory of the University of Michigan, using a Finnigan MAT Kiel IV preparation device coupled directly to the inlet of a Finnigan MAT 253 triple collector isotope ratio mass spectrometer. The international carbonate standard NBS-19 was used to calibrate to V-PDB, with an average precision of 0.15 ‰. The C-isotope analyses of the total organic fraction ( $\delta^{13}\text{C}_{\text{TOC}}$ ) were performed at the Stable Isotope Laboratory (SIDI) of the Universidad Autónoma of Madrid. Samples were treated with 3% HCL for 24 hours to remove carbonates and then analysed with an Carlo Erba 1108 elemental analyser coupled to a IRMS VG Isochrom in continuous flow mode. The results were calibrated to the VPDB standard, with a precision better than 0.1 ‰.

Samples for compound specific C-isotopes ( $\delta^{13}\text{C}_{\text{alg}}$ ) from Cau were extracted at the University of Jaén. Around 10 grams of grounded bulk sample was extracted using Dionex automated solvent extraction (ASE) and a mixture of dichloromethane (DCM) and methanol (MeOH) (8:2). The ASE program consisted of three 5 min cycles at 100 °C and 10 atm. The five samples from Djebel Serdj (Tunisia) were extracted at the University of Bristol using soxhlet apparatus. Between 30 and 40 grams of grounded bulk sample was extracted with a mixture of dichloromethane (DCM) and methanol (MeOH) (2:1) for 24 hrs. The total lipid extracts of samples from both locations were concentrated and separated into three fractions using silica open column chromatography. Successive elution with 3 ml of hexane, 4 ml hexane/DCM (9:1 v/v) and 4 ml of MeOH resulted in saturated hydrocarbon, aromatic and polar fractions, respectively. Compound specific  $\delta^{13}\text{C}$  values of the saturated hydrocarbons were determined using an Isoprime 100 GC-combustion-isotope ratio MS (GC-C-IRMS) system at the University of Bristol. Samples were measured in duplicate and  $\delta^{13}\text{C}$  values were converted to Vienna Pee Dee Belemnite (VPDB) by bracketing with an in-house gas ( $\text{CO}_2$ ) of known  $\delta^{13}\text{C}$  value. Instrument stability was monitored by regular analysis of an in-house fatty acid methyl ester standard mixture; long-term precision is  $\pm 0.3$  ‰. Injection volume was 2  $\mu\text{l}$  on to a Zebron-I non-polar column (50 m x 0.32 mm i.d., 0.10  $\mu\text{m}$  film thickness). The GC oven program was: 70 °C (1 min hold), to 130 °C at 20 °C/min, then to 300 °C at 4 °C/min, and a final hold for 25 minutes at 300 °C. Samples were automatically integrated using the IonVantage software package.

### $p\text{CO}_2$ calculations using compound specific $\delta^{13}\text{C}_{\text{alg}}$

Popp et al.<sup>30,31</sup> demonstrated that for several species of marine phytoplankton, and assuming that  $\text{CO}_2(\text{aq})$  enters the cell via diffusion only, which is likely during the high  $\text{CO}_2$  world of the Cretaceous<sup>32</sup>, the isotopic effect associated with the photosynthetic fixation of carbon ( $\epsilon_p$ ) depends on the concentration of  $\text{CO}_2(\text{aq})$ , growth rate, and cell geometry.

$$(1) \epsilon_p = \epsilon_f - \frac{b}{[\text{CO}_2(\text{aq})]}$$

With  $b$  being the combined species-specific factors that reflect physiological factors, including growth rate and cell geometry, and  $\epsilon_f$  being the maximum isotopic fractionation associated with the photosynthetic fixation of carbon, which is 25 ‰ for algae<sup>33</sup>.

Assuming surface waters were in equilibrium with the atmosphere, atmospheric  $p\text{CO}_2$  can be calculated using Henry's law:

$$(2) p\text{CO}_2(\text{ppmv}) = \frac{[\text{CO}_2(\text{aq})]}{K_o}$$

With  $K_o$ , the solubility constant, depending on temperature and salinity.

$$(3) \ln K_o (\text{moles/l/atm}) = A_1 + A_2 \frac{100}{T} + A_3 \ln \frac{T}{100} + S \left[ B_1 + B_2 \frac{T}{100} + B_3 \left( \frac{T}{100} \right)^2 \right]$$

With  $T$  = temperature (Kelvin),  $S$  = salinity (‰),  $A_1 = -58.0931$ ,  $A_2 = 90.5069$ ,  $A_3 = 22.2940$ ,  $B_1 = 0.027766$ ,  $B_2 = -0.025888$ ,  $B_3 = 0.0050578$ <sup>34</sup>

Based on this model, a large number of studies have used bulk organic matter ( $\delta^{13}\text{C}_{\text{TOC}}$ ) and compound specific  $\delta^{13}\text{C}$  values to calculate  $\epsilon_p$  and/or  $p\text{CO}_2$  throughout geological time<sup>35-39</sup>, including the Cretaceous and the OAEs<sup>6,10,22,24,40,41</sup>.

Here we calculated  $p\text{CO}_2$  using  $\delta^{13}\text{C}_{\text{alg}}$  based on four different marine biomarker lipids ( $\text{C}_{17}$  and  $\text{C}_{18}$   $n$ -alkanes and pristane and phytane) to generate a high resolution record from Cau and a low-resolution at Djebel Serdj. Biomarkers such as pristane and phytane, derived from phytol side chains of the chlorophylls of algae and cyanobacteria, are robust proxies for the isotopic composition of phytoplankton<sup>10,42</sup>.

$\epsilon_p$  depends on the isotopic difference between dissolved (aq)  $\text{CO}_2$  ( $\delta_d$ ) and primary photosynthate ( $\delta_p$ )<sup>40</sup>.

$$(4) \epsilon_p = 10^3 \left[ \frac{\delta_d + 1000}{\delta_p + 1000} - 1 \right]$$

We calculated the isotopic composition of primary photosynthate ( $\delta_p$ ) using the compound-specific isotopic composition ( $\delta^{13}\text{C}_{\text{alg}}$ ) and taking into the isotopic offset between biomarker lipids and biomass ( $\Delta\delta$ ), which is assumed to be 4 ‰ for pristane and phytane<sup>24,41-43</sup>. In our samples  $\delta^{13}\text{C}$  values of the short-chain  $n$ -alkanes are very similar to those of pristane and phytane (average offset 0.4 ‰), in-line with findings from other OAEs<sup>44</sup>, and we therefore assumed  $\Delta\delta$  to be 4 ‰ for all four compounds.

$$(5) \delta_p = \delta^{13}\text{C}_{\text{TOC}} = \delta^{13}\text{C}_{\text{alg}} + \Delta\delta = \delta^{13}\text{C}_{\text{alg}} + 4 \text{ ‰}$$

The isotopic composition of dissolved  $\text{CO}_2$  ( $\delta_d$ ) was calculated using the isotopic composition of bulk carbonate ( $\delta^{13}\text{C}_{\text{carb}}$ ), the calcite-bicarbonate enrichment of 1 ‰<sup>45</sup> and the temperature dependent carbon isotopic fractionation of dissolved  $\text{CO}_2$  with respect to  $\text{HCO}_3^-$  ( $\epsilon_{b(a)}$ )<sup>46</sup>.

$$(6) \delta_d = \delta^{13}\text{C}_{\text{carb}} - 1 + \epsilon_{b(a)}$$

$$(7) \epsilon_{b(a)} = 24.12 - \frac{9866}{T}$$

## Uncertainties in $p\text{CO}_2$ estimates

The absolute CO<sub>2</sub> values are calculated using a number of assumptions for palaeoproductivity, sea surface temperature, and equilibrium CO<sub>2</sub> exchange between ocean and atmosphere and should be considered as estimates. Below we discuss these assumptions and their impact on the absolute *p*CO<sub>2</sub> estimates. Importantly our main conclusions depend on the timing of changes in *p*CO<sub>2</sub> and are valid independent of the absolute CO<sub>2</sub> estimates or magnitude of change.

#### *Fidelity of the bulk $\delta^{13}\text{C}_{\text{carb}}$*

The first assumption is that bulk  $\delta^{13}\text{C}_{\text{carb}}$  at Cau reflects the isotopic composition of dissolved (aq) CO<sub>2</sub> ( $\delta_{\text{d}}$ ), which directly impacts  $\epsilon_{\text{p}}$  (see eq. 4 and 6). First, the  $\delta^{13}\text{C}$  composition of carbonate rocks is much more resistant to chemical overprinting than  $\delta^{18}\text{O}$ , such that even clearly diagenetically altered and dolomitized carbonates appear to preserve their original  $\delta^{13}\text{C}$  composition<sup>47</sup>, including OAE 1a sections<sup>48</sup>. In addition, nanofossil-dominated bulk carbonate  $\delta^{13}\text{C}$  is a reliable recorder of  $\delta^{13}\text{C}_{\text{DIC}}$  in pre-Cenozoic sediments<sup>49</sup> and  $\delta^{13}\text{C}_{\text{carb}}$  is well-suited for global correlation during OAEs<sup>3</sup>. As a result the shape of the  $\delta^{13}\text{C}_{\text{carb}}$  curves and magnitude of the positive and negative carbon isotope excursion across OAE 1a is similar across the globe (and in a range of depositional settings). In fact because black shale deposition is asynchronous, most authors use  $\delta^{13}\text{C}$  chemostratigraphy and the C-isotope segments defined by Menegatti et al.<sup>23</sup> to correlate OAE 1a records across the globe<sup>1,14,15,48,50</sup>. Published  $\delta^{13}\text{C}_{\text{carb}}$  records may appear different in shape and magnitude but this apparent difference between sections is to a large extent due to visual comparison of expanded to condensed sections.

To demonstrate that our  $\delta^{13}\text{C}_{\text{carb}}$  record from Cau is similar in shape and magnitude of excursions to other records, we compare the record from Cau to the  $\delta^{13}\text{C}_{\text{carb}}$  of a similarly expanded section from southeast France<sup>16</sup> (Fig. S1). The reason for choosing this record is that it is one of the few other expanded OAE 1a sections. We subsequently tuned the  $\delta^{13}\text{C}_{\text{carb}}$  from SE France record to the one from Cau other using four tie-points. Three are based on biostratigraphy and one on the boundary of the C4/C5-isotope segment. Figure S2 clearly demonstrates the similarity in shape and magnitude of excursion of the two  $\delta^{13}\text{C}_{\text{carb}}$  curves. The similarity between the two  $\delta^{13}\text{C}_{\text{carb}}$  curves, located around 1000 km apart, suggests that the  $\delta^{13}\text{C}_{\text{carb}}$  record from Cau is not significantly influenced by diagenesis or other secondary effects but reflects a  $\delta^{13}\text{C}_{\text{DIC}}$  signal and can be used to calculate  $\delta_{\text{d}}$ . Even so, we assume a 0.5 ‰ uncertainty in this in our uncertainty estimates (see further below).

#### *Changes in algal composition and physiology*

Changes in the algal composition or physiology can affect  $\delta^{13}\text{C}_{\text{alg}}$  and  $\delta^{13}\text{C}_{\text{TOC}}$  and hence ultimately our *p*CO<sub>2</sub> estimates. To assess whether these factors changed across OAE 1a at Cau, we determined the relative C<sub>27</sub>-C<sub>30</sub>  $\alpha\alpha\alpha\text{R}$  sterane distribution in all samples. Steranes are derived from algal-derived steroids and sterols, such that their relative distribution in the geological record is often used to infer changes in algal composition<sup>51,52</sup>. In addition, the sterol, and hence sterane, composition can be influenced by environmental factors such as light intensity, temperature, and growth stage<sup>53</sup>.

Our results show that the sterane distribution varied little across OAE 1a and changes do not coincide with major changes in  $\delta^{13}\text{C}$  (Fig. S3). This provides strong evidence against significant changes in algal composition and/or environmental factors at Cau during OAE 1a influencing  $\delta^{13}\text{C}$ . This is in-line with the lack of a temperature change in the low-latitudes during OAE 1a as indicated by our TEX<sub>86</sub>

estimates from Site 398, as well as the minimal change in TOC content (Fig. S4). Taken together, changes in algal composition and/or variations in physiology due to changing environmental factors are unlikely to have had a significantly effect. Although more tentative, the lack of any change in algal assemblage suggests that there were no dramatic changes in the nutrient contents of the waters, mitigating concerns associated with growth rate impacts on  $\delta^{13}\text{C}$  records.

#### *Comparison to published records of $\delta^{13}\text{C}_{\text{alg}}$ and $\epsilon_p$*

The  $\delta^{13}\text{C}_{\text{alg}}$  from Cau (as well as Djebel Serdj, Fig. S8) are similar to those reported from other (low-resolution) sections across OAE 1a. Van Breugel et al.<sup>11</sup> provide  $\delta^{13}\text{C}$  of pristane across part of OAE 1a at Cismon. Their values range between -28 and -35 ‰, similar to the values we measured at Cau (-29 to -34.5 ‰ for pristane) and low-resolution record of Djebel Serdj (-29.2 to -32.6 ‰ for pristane). For the last  $\pm 50$  Myr, numerous biomarker-based  $p\text{CO}_2$  records are based on  $\delta^{13}\text{C}$  of alkenones<sup>35,37</sup>. Although alkenones are generally not found in Cretaceous sediments, the first occurrence of alkenones actually is in the extremely organic rich OAE 1a section at Shatsky Rise (ODP Site 1213)<sup>54</sup>. The isotopic composition of these alkenones was determined in one sample ( $\sim -32$  ‰)<sup>55</sup>, similar to the minimum values we determined, and again demonstrate that the  $\delta^{13}\text{C}_{\text{alg}}$  we report are typical for OAE 1a.

None of these studies calculated  $\epsilon_p$ . At Shatsky, no  $\delta^{13}\text{C}_{\text{carb}}$  is available. Cismon is characterized by large variations in the source of organic matter<sup>11</sup> and  $\text{TEX}_{86}$  is influenced by thermal maturity<sup>56</sup>. Heimhofer et al.<sup>10</sup> used, among others,  $\text{C}_{17}$  and  $\text{C}_{18}$  short-chain *n*-alkanes to reconstruct  $\epsilon_p$  across segment C5 to C7 in the Serre Chaitieu section from France (Fig. S6). For this part of OAE 1a the  $\delta^{13}\text{C}$  of the short-chain *n*-alkanes in the Serre Chaitieu section ranges between -32 and -27 ‰, similar to our estimates for these compounds across segments C5-C7 at Cau (-32 to -25 ‰) and low-resolution record of Djebel Serdj (-27.9 to -31.8 ‰). Their estimates of  $\epsilon_p$ , although not depicting the increase in  $p\text{CO}_2$  as there are no data from segments C3 and C4, with maximum  $\epsilon_p$  values of around 22‰ are very similar to our maximum  $\epsilon_p$  values across this period (maximum  $\epsilon_p$  at Cau and Djebel Serdje are  $\sim 22$ ‰ during C4-C6), markedly higher than any values yet to be reported for the last 15 million years<sup>35</sup>. We therefore conclude that our  $\delta^{13}\text{C}_{\text{alg}}$  and  $\epsilon_p$  estimates are typical for OAE 1a, and reflect a global signal.

#### *Estimating the $b$ -value*

The growth rate and cell geometry impact the isotopic effect expressed during the photosynthetic fixation of carbon ( $\epsilon_p$ )<sup>31,33</sup>. These effects are combined into the constant  $b$  and have an impact on the absolute  $p\text{CO}_2$  estimates. In the modern ocean,  $b$  for haptophyte algae ranges from  $< 100$  in oligotrophic regions to  $> 200$  in upwelling regions<sup>33,57-59</sup>.

Although it is not straightforward to estimate  $b$  during OAE 1a, previous estimates for the Late Cretaceous and OAE 2 assumed a value of 171<sup>24,41,43</sup>. This value is based on the proposed linear correlated between  $b$  and sedimentary bulk  $\delta^{15}\text{N}$  values<sup>57</sup> and an assumed  $\delta^{15}\text{N}$  of -2 ‰ during the Late Cretaceous at Demerara rise<sup>41</sup>.

$$(8) \ b = 53.27 \left[ \frac{\delta^{15}\text{N} - 12.386}{-8.146} \right] + 77.21$$

Bulk  $\delta^{15}\text{N}$  values across OAE 1a yield similar negative values between -1 and -3 ‰<sup>50,60</sup>, also suggesting a  $b$  value of  $\sim 171$ . This relationship is implicitly based on

modern ocean alkenone  $\delta^{13}\text{C}$  values and therefore is tuned for coccolithophorids; algae with different surface area to volume ratios or even different membrane diffusivity could have different  $b$  values<sup>61</sup>. This represents a first order limitation on the calculation of absolute  $p\text{CO}_2$  values. Nonetheless, Popp et al.<sup>31</sup> have shown that other photoautotrophs do exhibit similar relationships; as such, we can assume a constant  $b$  value of 171 for our  $p\text{CO}_2$  estimates but use a range of  $b$  values to constrain the uncertainty of the absolute values. Given the lack of evidence for changes in the algal community structure, we suggest that this has had minimal impact on our temporal trends.

Cau was not an upwelling site and is characterized by background TOC values between 0.5 and 1.5 %. Even during OAE 1a the period of increased organic matter burial was short lived and not very intense as indicated by the moderate and brief increase in TOC to maximum values of 2.5 % (Fig. S4), making it unlikely that the  $b$  value was much higher. If  $b$  did increase, then this would have occurred during segments C3-C6 and accounting for it would yield higher  $p\text{CO}_2$  estimates at this time.

#### *Estimating subtropical Sea Surface Temperatures (SSTs)*

Sea surface temperatures (SSTs) impact the estimated  $p\text{CO}_2$  in several ways, but predominantly from their influence on Henry's Law. Here we estimated SSTs using the  $\text{TEX}_{86}$  palaeothermometer, which is based on the distribution of isoprenoidal glycerol dialkyl glycerol tetraethers (GDGTs) in marine sediments<sup>62,63</sup>. The advantage of  $\text{TEX}_{86}$  over inorganic geochemical proxies is that  $\text{TEX}_{86}$  is less influenced by diagenesis, which for example can alter the primary  $\delta^{18}\text{O}$  signature of carbonates, and is not directly controlled by seawater chemistry such as  $\text{Mg}/\text{Ca}$  and  $\delta^{18}\text{O}$ , which very likely was different during the Cretaceous and especially OAEs.

We did not detect measurable amounts of GDGTs in the samples from Cau. Although the organic matter at Cau is thermally immature<sup>20</sup> with respect to oil generation, this is not necessarily the case with respect to the occurrence of GDGTs. Due to the presence of heteroatoms (i.e. the ether bond), GDGTs begin to degrade at relatively low thermal maturity<sup>64,65</sup>; in fact, they are uncommon in the maturation window when steranes, pristane and phytane have begun to be liberated from kerogen.

To overcome this issue, we obtained  $\text{TEX}_{86}$ -based SST estimates from DSDP Site 398 across OAE 1a. Site 398 is located in the North Atlantic, slightly north of Cau (Fig. 1), and covers OAE 1a<sup>14</sup>. Importantly it contains abundant GDGTs. Using the  $\text{TEX}_{86}^{\text{H}}$ -calibration<sup>66</sup>, SSTs at Site 398 across OAE 1a (C3-C6) are remarkably warm and stable with values around 34.5 °C (Fig. S5c). Such high subtropical SSTs are consistent with a large range of proxy-evidence that indicates that the Cretaceous was characterized by a hot greenhouse climate<sup>67-70</sup>. In addition, it closely ties-in with recent  $\text{TEX}_{86}^{\text{H}}$  estimates across OAE 1a from the mid-latitudes (~39 °N palaeolatitude) that range between 30 and 33 °C<sup>2</sup>, tropical SSTs in the Pacific that range between 31 and 38 °C during OAE 1a<sup>63,71</sup>, and high-latitude Southern Ocean (~55 °N palaeolatitude) SSTs of around 28 °C during OAE 1a<sup>69</sup>, which all indicate very high SSTs during OAE 1a with SSTs > 30 °C extending far into the mid-latitudes.

BIT-values, a proxy for the input of soil derived GDGTs<sup>72</sup>, vary between 0.06 and 0.41 and there is no correlation between BIT-values and SSTs, arguing against a significant influence of terrestrial GDGTs on the  $\text{TEX}_{86}^{\text{H}}$  estimates. The organic matter at Site 398 across OAE 1a is thermally immature as indicated by the  $\text{C}_{31}$  hopane  $\beta\beta/(\beta\beta+\beta\alpha+\alpha\beta)$  ratios that are always greater than 0.5 (Fig. S5d).

The reconstructed SSTs from Site 398 indicate a stable and warm subtropical climate, which appears inherent to greenhouse climates<sup>73</sup>. Based on the record from

Site 398, we assumed that subtropical SSTs across OAE 1a were relatively stable at Cau at 34.5 °C. Higher (36°C) or lower (30°C) SST estimates would lead to slightly different (max 250 ppmv) CO<sub>2</sub> values (Fig. S6). Assuming an increase in SSTs across OAE 1a, as seen in the higher latitudes<sup>2</sup>, would result in a slightly more pronounced increase in pCO<sub>2</sub> across OAE 1a.

### *Uncertainty envelopes*

As explained above, our best pCO<sub>2</sub> estimates assume a *b*-value of 171, that δ<sup>13</sup>C<sub>carb</sub> reflects seawater δ<sup>13</sup>C<sub>DIC</sub>, and that SSTs in the subtropics were 34.5 °C. Assuming these parameters, pCO<sub>2</sub> was calculated for, where possible, all four biomarkers and an average of these estimates was plotted in figure 3 as a black line with orange data points.

To accurately incorporate the main sources of uncertainty in our pCO<sub>2</sub> calculations, largely associated with δ<sup>13</sup>C<sub>DIC</sub> determinations from δ<sup>13</sup>C<sub>carb</sub> that has an impact on ε<sub>p</sub> and uncertainty in the *b*-value due to growth rate and cell physiology that influences the absolute pCO<sub>2</sub> estimates, we calculated a minimum and maximum pCO<sub>2</sub> scenario. The minimum scenario assumes that δ<sup>13</sup>C<sub>carb</sub> overestimates seawater δ<sup>13</sup>C<sub>DIC</sub> by 0.5 ‰ and a low-end *b*-value of 150. The maximum scenario assumes that δ<sup>13</sup>C<sub>carb</sub> underestimates seawater δ<sup>13</sup>C<sub>DIC</sub> by 0.5 ‰ and a high-end *b*-value of 200. Note that uncertainty in δ<sup>13</sup>C<sub>carb</sub> manifest in ε<sub>p</sub>, which at Cau is similar compared to previous estimates<sup>10</sup> and other sites. A range from 150 to 200 for *b* was chosen as both Cau and Djebel Serdje are not upwelling sites and not characterized by large variations in TOC content or changes in algal composition and physiology. Assuming these parameters, pCO<sub>2</sub> was calculated for all four biomarkers. In figures 3 and S8, the orange shading represents the spread between the minimum and maximum pCO<sub>2</sub> estimates and, again, is the average value of all biomarker measurements (see Fig. S7). The light yellow shading represents the analytical uncertainty related to the compound specific δ<sup>13</sup>C measurements (e.g., how well does the average value of the four biomarkers represent the spread in compound specific δ<sup>13</sup>C) and represents 1σ from the average min. and max. pCO<sub>2</sub>-scenario (e.g. 1σ from the orange shading).

The uncertainty in Δ<sup>13</sup>C (the turquoise shading in figure 3), was calculated assuming both δ<sup>13</sup>C<sub>carb</sub> and δ<sup>13</sup>C<sub>TOC</sub> were as much as 0.5 ‰ too high or too low compared to seawater δ<sup>13</sup>C<sub>DIC</sub> and primary photosynthate δ<sup>13</sup>C, respectively, resulting in a combined error of 0.71 ‰ ( $\sqrt{(0.5^2+0.5^2)}$ ).

### **Duration of isotope segment C3**

Following Menegatti et al.<sup>23</sup> we defined C3 to span the decrease in bulk δ<sup>13</sup>C<sub>carb</sub>, covering the interval between 46 and 62 meter in our section (Fig. 2a). Identical to other OAE 1a records<sup>5,15,16</sup> the onset of the nannoconid crisis precedes the beginning of C3 at Cau. The first occurrence of *Schackoina cabri* at the top of C3 corresponds to what has been observed in other expanded sections<sup>16,17</sup>.

Previous estimates for the duration of C3 range from 20 to 45 kyr at Cismon<sup>14,15</sup>. However results from other more expanded sections demonstrate that this interval in Cismon is (highly) condensed and the duration of C3 was likely longer, with ranges between 100 and 300 kyr<sup>16,17,74,75</sup>. Recently the C3 interval at Cismon was also redefined, with an updated duration of between 100 and 200 kyr<sup>56</sup>.

### **Duration of the reconstructed CO<sub>2</sub> input at Cau**

Even assuming a minimal duration of 20-45 ka for C3 as suggested by the original Cismon estimates<sup>14,15</sup>, the reconstructed CO<sub>2</sub> increase at Cau occurs across the later

part of C3 as well as the majority of C4, which lasted  $239 \pm 39$  kyr at Cismon<sup>15</sup>. This implies that independent of the exact duration of C3, the CO<sub>2</sub> increase occurred over at least 100 ka. Assuming a more likely duration of C3 of 100 to 300 kyr together with the duration of C4 of 239 ka, implies that the CO<sub>2</sub> increase at Cau likely occurred over more than 300 ka.

### Correlations to Cau

We used the carbon isotope segment chemostratigraphy, originally developed by Menegatti et al.<sup>23</sup>, to compare the *p*CO<sub>2</sub> record from Djebel Serdj and Os-isotope record from Cismon to the records from Cau. For Cismon we used the updated definition of isotope segment C3 as used in Bottini et al.<sup>56</sup>. For the timing of the nanoconid crisis at Cismon we used the definition given in Malinverno et al.<sup>15</sup>. For Djebel Serdj we redefined the carbon isotope segments as shown in Figure S8, largely following Heldt et al.<sup>26</sup>. The low-resolution *p*CO<sub>2</sub> estimates from Djebel Serdj were plotted on top of those of Cau using a direct correlation. So for example, the estimates from the middle of segment C3 at Djebel Serdj are shown in the middle of C3 at Cau. The vertical error bars on the *p*CO<sub>2</sub> estimates from Djebel Serdj as shown in figure 3 represents the uncertainty in this correlation.

### References:

- 30 Popp, B. N., Takigiku, R., Hayes, J. M., Louda, J. W. & Baker, E. W. The post-Paleozoic chronology and mechanism of <sup>13</sup>C depletion in primary marine organic matter. *Am. J. Sc.* **289**, 436-454 (1989).
- 31 Popp, B. N. *et al.* Effect of Phytoplankton Cell Geometry on Carbon Isotopic Fractionation. *Geochim. Cosmochim. Ac.* **62**, 69-77 (1998).
- 32 Laws, E. A., Popp, B. N., Cassar, N. & Tanimoto, J. <sup>13</sup>C discrimination patterns in oceanic phytoplankton: likely influence of CO<sub>2</sub> concentrating mechanisms, and implications for palaeoreconstructions. *Funct. Plant Biol.* **29**, 323-333 (2002).
- 33 Bidigare, R. R. *et al.* Consistent fractionation of <sup>13</sup>C in nature and in the laboratory: Growth-rate effects in some haptophyte algae. *Global Biogeochem. Cy.* **11**, 279-292 (1997).
- 34 Weiss, R. F. Carbon dioxide in water and seawater: the solubility of a non-ideal gas. *Mar. Chem.* **2**, 203-215 (1974).
- 35 Pagani, M., Zachos, J. C., Freeman, K. H., Tipple, B. & Bohaty, S. Marked Decline in Atmospheric Carbon Dioxide Concentrations During the Paleogene. *Science* **309**, 600-603 (2005).
- 36 Schoon, P. L., Sluijs, A., Sinninghe Damsté, J. S. & Schouten, S. Stable carbon isotope patterns of marine biomarker lipids in the Arctic Ocean during Eocene Thermal Maximum 2. *Paleoceanography* **26**, PA3215 (2011).
- 37 Seki, O. *et al.* Alkenone and boron-based Pliocene *p*CO<sub>2</sub> records. *Earth Plant. Sc. Lett.* **292**, 201-211 (2010).
- 38 Badger, M. P. S. *et al.* CO<sub>2</sub> drawdown following the middle Miocene expansion of the Antarctic Ice Sheet. *Paleoceanography* **28**, 42-53 (2013).
- 39 Raymo, M. E., Grant, B., Horowitz, M. & Rau, G. H. Mid-Pliocene warmth: stronger greenhouse and stronger conveyor. *Mar. Micropaleontol.* **27**, 313-326 (1996).
- 40 Freeman, K. H. & Hayes, J. M. Fractionation of carbon isotopes by phytoplankton and estimates of ancient CO<sub>2</sub> levels. *Global Biogeochem. Cy.* **6**, 185-198 (1992).

656 41 Bice, K. L. *et al.* A multiple proxy and model study of Cretaceous upper ocean  
657 temperatures and atmospheric CO<sub>2</sub> concentrations. *Paleoceanography* **21**,  
658 PA2002 (2006).

659 42 Schouten, S. *et al.* Biosynthetic effects on the stable carbon isotopic  
660 compositions of algal lipids: implications for deciphering the carbon isotopic  
661 biomarker record. *Geochim. Cosmochim. Ac.* **62**, 1397-1406 (1998).

662 43 van Bentum, E. C., Reichart, G. J., Forster, A. & Sinninghe Damsté, J. S.  
663 Latitudinal differences in the amplitude of the OAE-2 carbon isotopic  
664 excursion: pCO<sub>2</sub> and paleo productivity. *Biogeosciences* **9**, 717-731 (2012).

665 44 Schouten, S., van Kaam-Peters, H. M. E., Rijpstra, W. I. C., Schoell, M. &  
666 Sinninghe Damsté, J. S. Effects of an oceanic anoxic event on the stable  
667 carbon isotopic composition of early Toarcian carbon. *Am. J. Sci.* **300**, 1-22  
668 (2000).

669 45 Romanek, C. S., Grossman, E. L. & Morse, J. W. Carbon isotopic  
670 fractionation in synthetic aragonite and calcite: Effects of temperature and  
671 precipitation rate. *Geochim. Cosmochim. Ac.* **56**, 419-430 (1992).

672 46 Mook, W. G., Bommerson, J. C. & Staverman, W. H. Carbon isotope  
673 fractionation between dissolved bicarbonate and gaseous carbon dioxide.  
674 *Earth Plant. Sc. Lett.* **22**, 169-176 (1974).

675 47 Halverson, G. P., Hoffman, P. F., Schrag, D. P., Maloof, A. C. & Rice, A. H.  
676 N. Toward a Neoproterozoic composite carbon-isotope record. *Geol. Soc. Am.*  
677 *Bull.* **117**, 1181-1207 (2005).

678 48 Jenkyns, H. C. in *Proceedings of the Ocean Drilling Program, Scientific*  
679 *Results, vol. 143* (eds E.L. Winterer, W.W. Sager, J.V. Firth, & J.M. Sinton)  
680 99-104 (Ocean Drilling Program, 1995).

681 49 Stoll, H. M. Limited range of interspecific vital effects in coccolith stable  
682 isotopic records during the Paleocene-Eocene thermal maximum.  
683 *Paleoceanography* **20**, PA1007 (2005).

684 50 Dumitrescu, M. & Brassell, S. C. Compositional and isotopic characteristics of  
685 organic matter for the early Aptian Oceanic Anoxic Event at Shatsky Rise,  
686 ODP Leg 198. *Palaeogeogr., Palaeoclimatol., Palaeoecol.* **235**, 168-191  
687 (2006).

688 51 Grantham, P. J. & Wakefield, L. L. Variations in the sterane carbon number  
689 distributions of marine source rock derived crude oils through geological time.  
690 *Org. Geochem.* **12**, 61-73 (1988).

691 52 Schwark, L. & Empt, P. Sterane biomarkers as indicators of palaeozoic algal  
692 evolution and extinction events. *Palaeogeogr., Palaeoclimatol., Palaeoecol.*  
693 **240**, 225-236 (2006).

694 53 Volkman, J. Sterols in microorganisms. *Appl Microbiol Biotechnol* **60**, 495-  
695 506 (2003).

696 54 Brassell, S. C. & Dumitrescu, M. Recognition of alkenones in a lower Aptian  
697 porcellanite from the west-central Pacific. *Org. Geochem.* **35**, 181-188 (2004).

698 55 Dumitrescu, M. & Brassell, S. C. Biogeochemical assessment of sources of  
699 organic matter and paleoproductivity during the early Aptian Oceanic Anoxic  
700 Event at Shatsky Rise, ODP Leg 198. *Org. Geochem.* **36**, 1002-1022 (2005).

701 56 Bottini, C. *et al.* Climate variability and ocean fertility during the Aptian Stage.  
702 *Clim. Past* **11**, 383-402 (2015).

703 57 Andersen, N., Müller, P. J., Kirst, G. & Schneider, R. R. in *Use of Proxies in*  
704 *Paleoceanography* (eds Gerhard Fischer & Gerold Wefer) Ch. 19, 469-488  
705 (Springer Berlin Heidelberg, 1999).



706 58 Schulte, S., Benthien, A., Andersen, N., Müller, P. J. & Schneider, R. in *The*  
707 *South Atlantic in the Late Quaternary: Reconstruction of Material Budget and*  
708 *Current Systems* (eds G. Wefer, S. Mulitza, & V. Ratmeyer) 195-211  
709 (Springer, 2003).

710 59 Pagani, M. The Alkenone-CO<sub>2</sub> Proxy and Ancient Atmospheric Carbon  
711 Dioxide. *Philos. T. Roy. Soc. A*. **360**, 609-632 (2002).

712 60 Kuypers, M. M. M., van Breugel, Y., Schouten, S., Erba, E. &  
713 Sinninghe Damsté, J. S. N<sub>2</sub>-fixing cyanobacteria supplied nutrient N for  
714 Cretaceous oceanic anoxic events. *Geology* **32**, 853-856 (2004).

715 61 Pancost, R. D. *et al.* Reconstructing Late Ordovician carbon cycle variations.  
716 *Geochim. Cosmochim. Ac.* **105**, 433-454 (2013).

717 62 Schouten, S., Hopmans, E. C., Schefuss, E. & Sinninghe Damsté, J. S.  
718 Distributional variations in marine crenarchaeotal membrane lipids: a new tool  
719 for reconstructing ancient sea water temperatures? *Earth Plant. Sc. Lett.* **204**,  
720 265-274 (2002).

721 63 Schouten, S. *et al.* Extremely high sea-surface temperatures at low latitudes  
722 during the middle Cretaceous as revealed by archaeal membrane lipids.  
723 *Geology* **31**, 1069-1072 (2003).

724 64 Schouten, S., Hopmans, E. C. & Sinninghe Damsté, J. S. The effect of  
725 maturity and depositional redox conditions on archaeal tetraether lipid  
726 palaeothermometry. *Org. Geochem.* **35**, 567-571 (2004).

727 65 Schouten, S., Hopmans, E. C. & Sinninghe Damsté, J. S. The organic  
728 geochemistry of glycerol dialkyl glycerol tetraether lipids: A review. *Org.*  
729 *Geochem.* **54**, 19-61 (2013).

730 66 Kim, J.-H. *et al.* New indices and calibrations derived from the distribution of  
731 crenarchaeal isoprenoid tetraether lipids: Implications for past sea surface  
732 temperature reconstructions. *Geochim. Cosmochim. Ac.* **74**, 4639-4654 (2010).

733 67 Littler, K., Robinson, S. A., Bown, P. R., Nederbragt, A. J. & Pancost, R. D.  
734 High sea-surface temperatures during the Early Cretaceous Epoch. *Nature*  
735 *Geosci.* **4**, 169-172 (2011).

736 68 Jenkyns, H. C., Forster, A., Schouten, S. & Sinninghe Damsté, J. S. High  
737 temperatures in the Late Cretaceous Arctic Ocean. *Nature* **432**, 888-892  
738 (2004).

739 69 Jenkyns, H. C., Schouten-Huibers, L., Schouten, S. & Sinninghe Damsté, J. S.  
740 Warm Middle Jurassic-Early Cretaceous high-latitude sea-surface  
741 temperatures from the Southern Ocean. *Clim. Past* **8**, 215-226 (2012).

742 70 Tarduno, J. A. *et al.* Evidence for Extreme Climatic Warmth from Late  
743 Cretaceous Arctic Vertebrates. *Science* **282**, 2241-2243 (1998).

744 71 Dumitrescu, M., Brassell, S. C., Schouten, S., Hopmans, E. C. &  
745 Sinninghe Damsté, J. S. Instability in tropical Pacific sea-surface temperatures  
746 during the early Aptian. *Geology* **34**, 833-836 (2006).

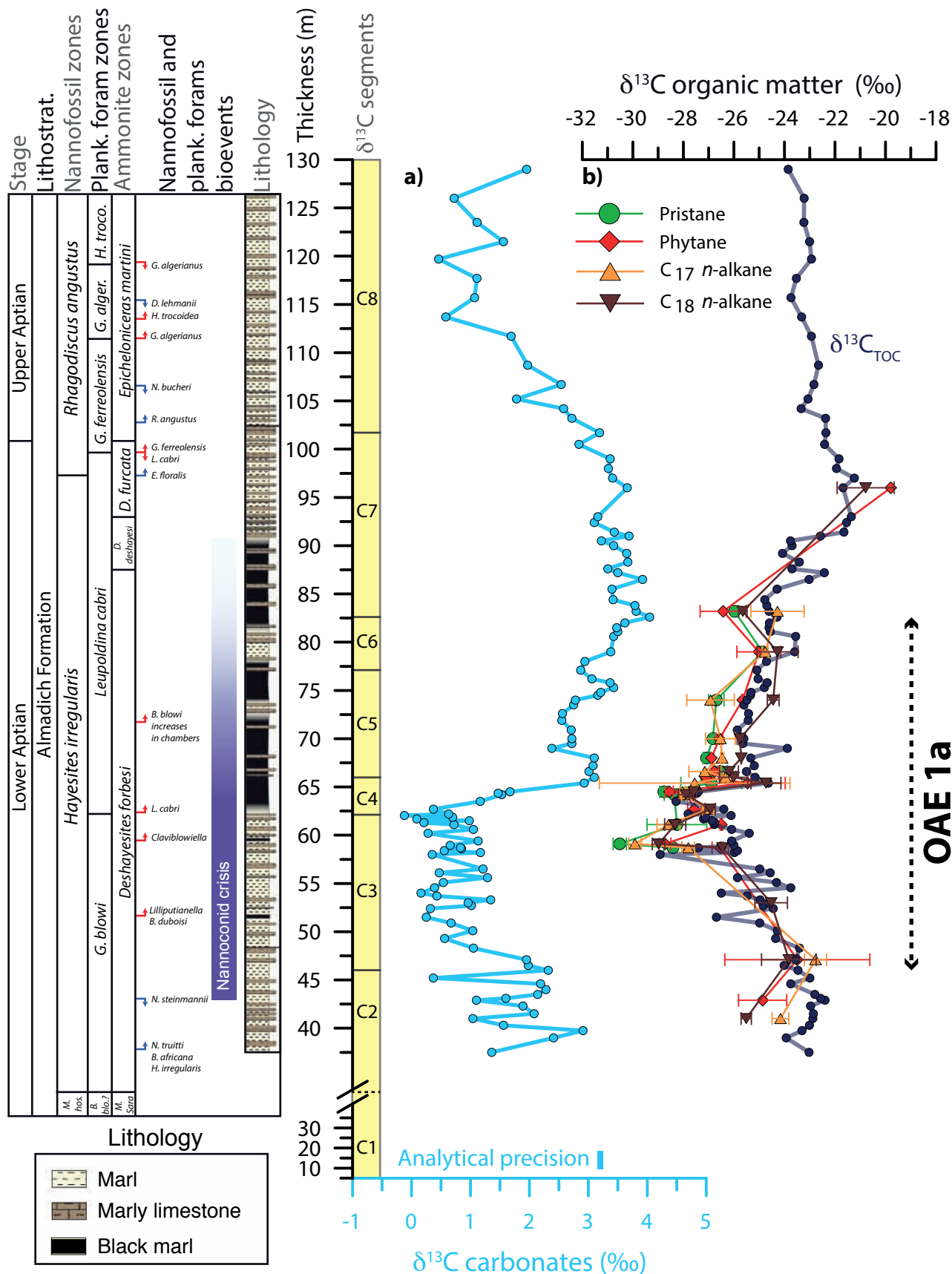
747 72 Hopmans, E. C. *et al.* A novel proxy for terrestrial organic matter in sediments  
748 based on branched and isoprenoid tetraether lipids. *Earth Plant. Sc. Lett.* **224**,  
749 107-116 (2004).

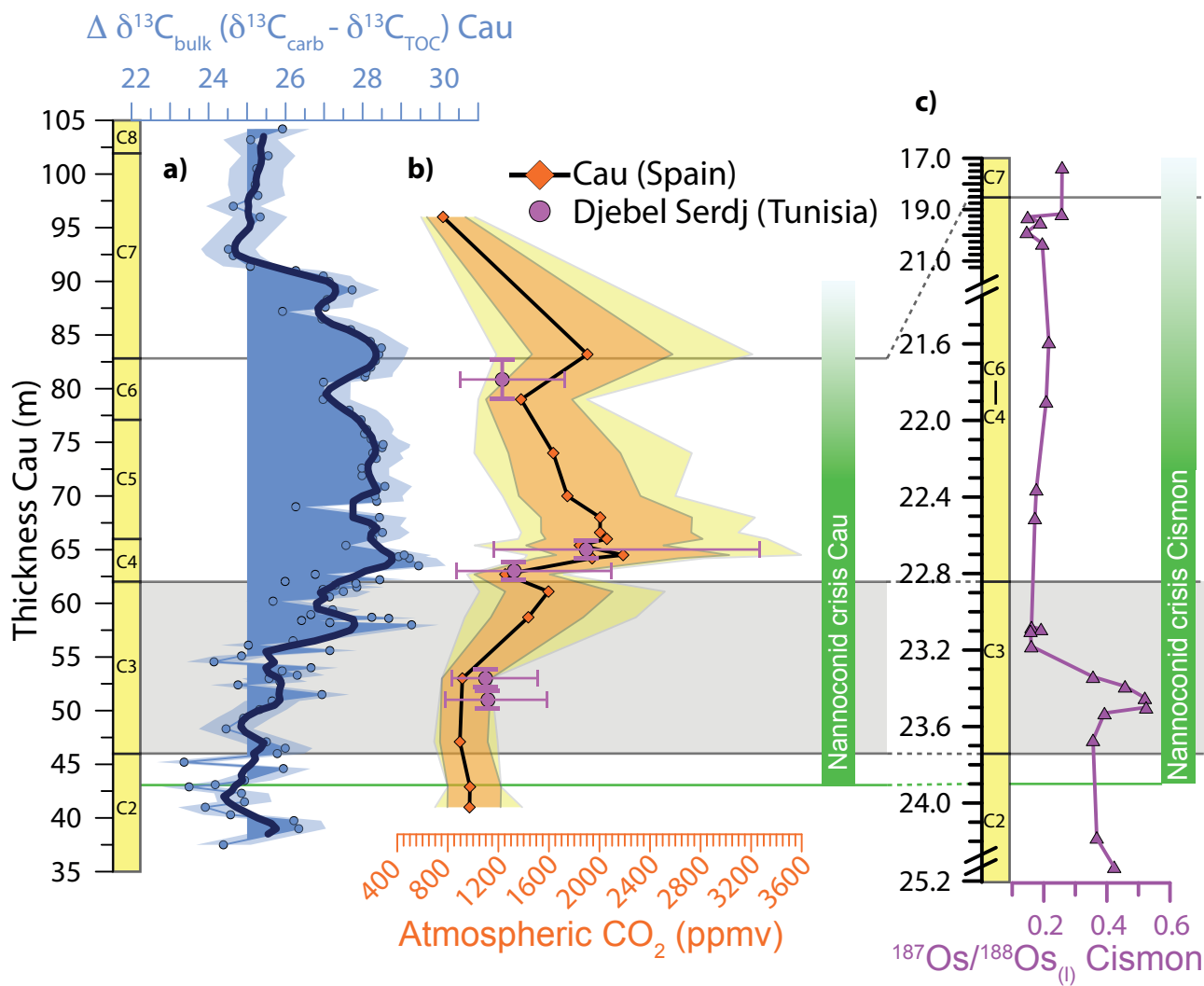
750 73 Pearson, P. N. *et al.* Stable warm tropical climate through the Eocene Epoch.  
751 *Geology* **35**, 211-214 (2007).

752 74 Hu, X., Zhao, K., Yilmaz, I. O. & Li, Y. Stratigraphic transition and  
753 palaeoenvironmental changes from the Aptian oceanic anoxic event 1a  
754 (OAE1a) to the oceanic red bed 1 (ORB1) in the Yenicesihlar section, central  
755 Turkey. *Cretaceous Res.* **38**, 40-51 (2012).

756 75 Huck, S., Heimhofer, U., Rameil, N., Bodin, S. & Immenhauser, A. Strontium  
757 and carbon-isotope chronostratigraphy of Barremian–Aptian shoal-water  
758 carbonates: Northern Tethyan platform drowning predates OAE 1a. *Earth*  
759 *Plant. Sc. Lett.* **304**, 547-558 (2011).  
760  
761







# Gradual and sustained carbon dioxide release during Aptian Oceanic Anoxic

## Event 1a

### Supplementary figures

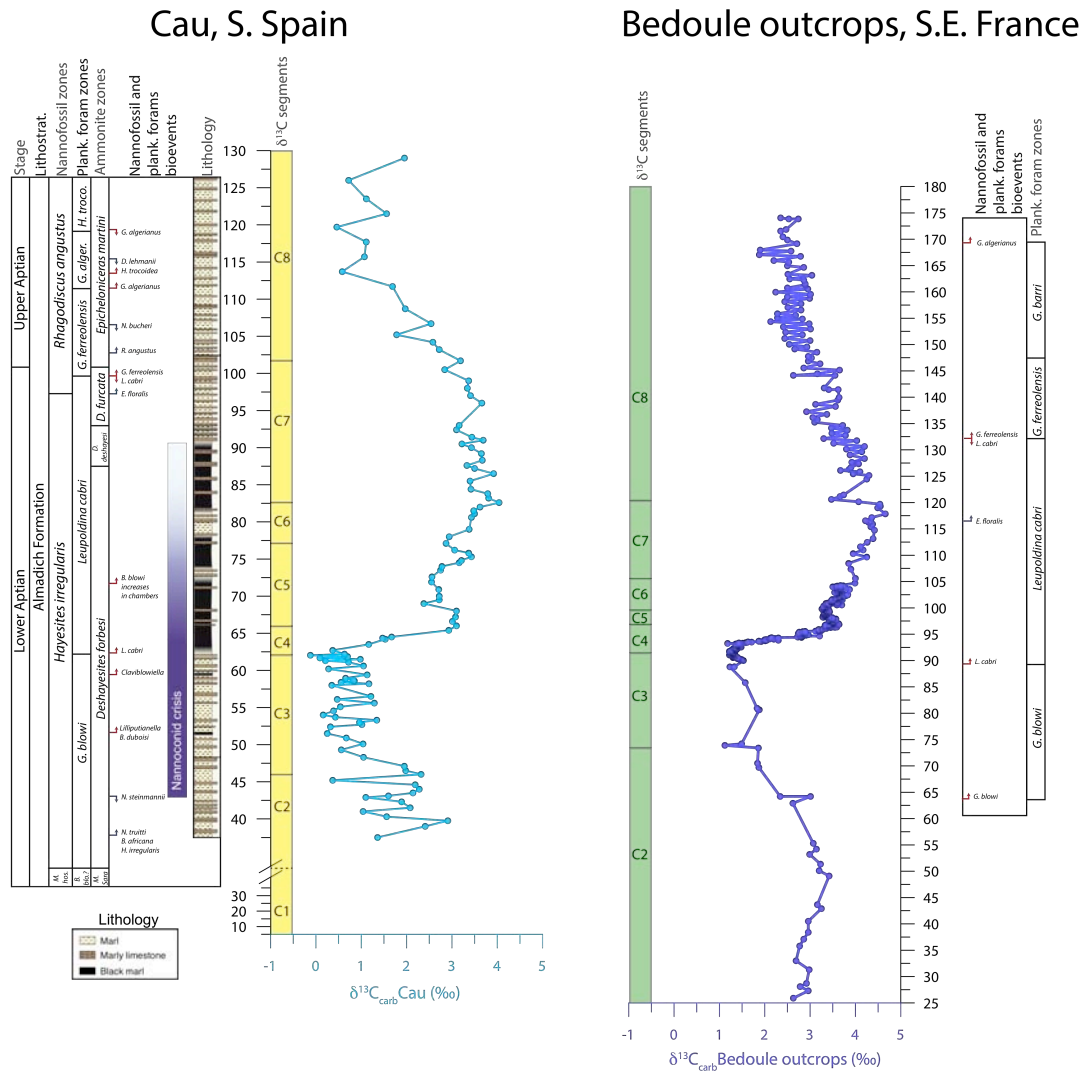


**Figure S1: Comparison of  $\delta^{13}\text{C}_{\text{carb}}$  records 1**  
 $\delta^{13}\text{C}_{\text{carb}}$  data from Cau (left) and SE France (right)<sup>S1</sup> on their individual depth scales and published biostratigraphy.

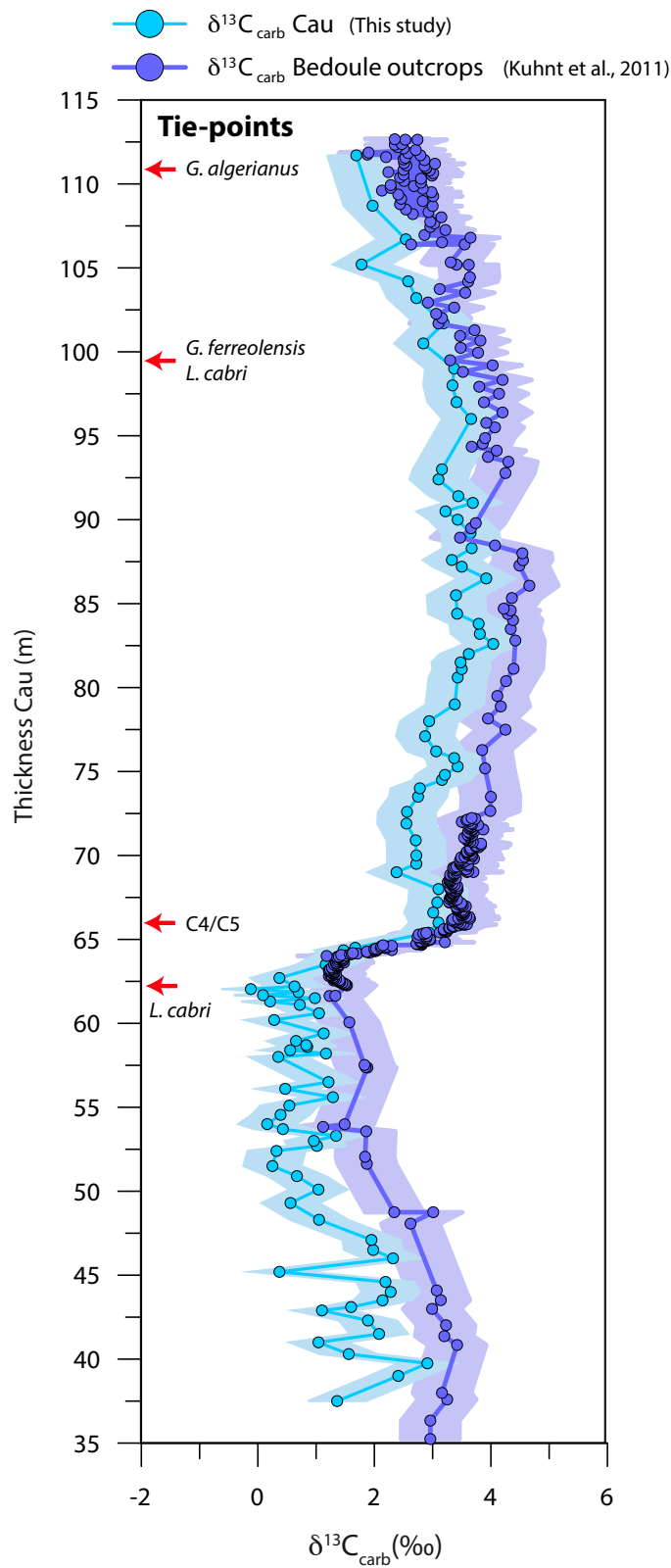


**Figure S2: Comparison of  $\delta^{13}\text{C}_{\text{carb}}$  records 2**

$\delta^{13}\text{C}_{\text{carb}}$  data from SE France<sup>SI</sup> tuned to Cau using a minimal of four tie-points (indicated by red arrows) to demonstrate the similarity in structure and magnitude of change. Shaded areas represent 0.5 ‰ uncertainty.

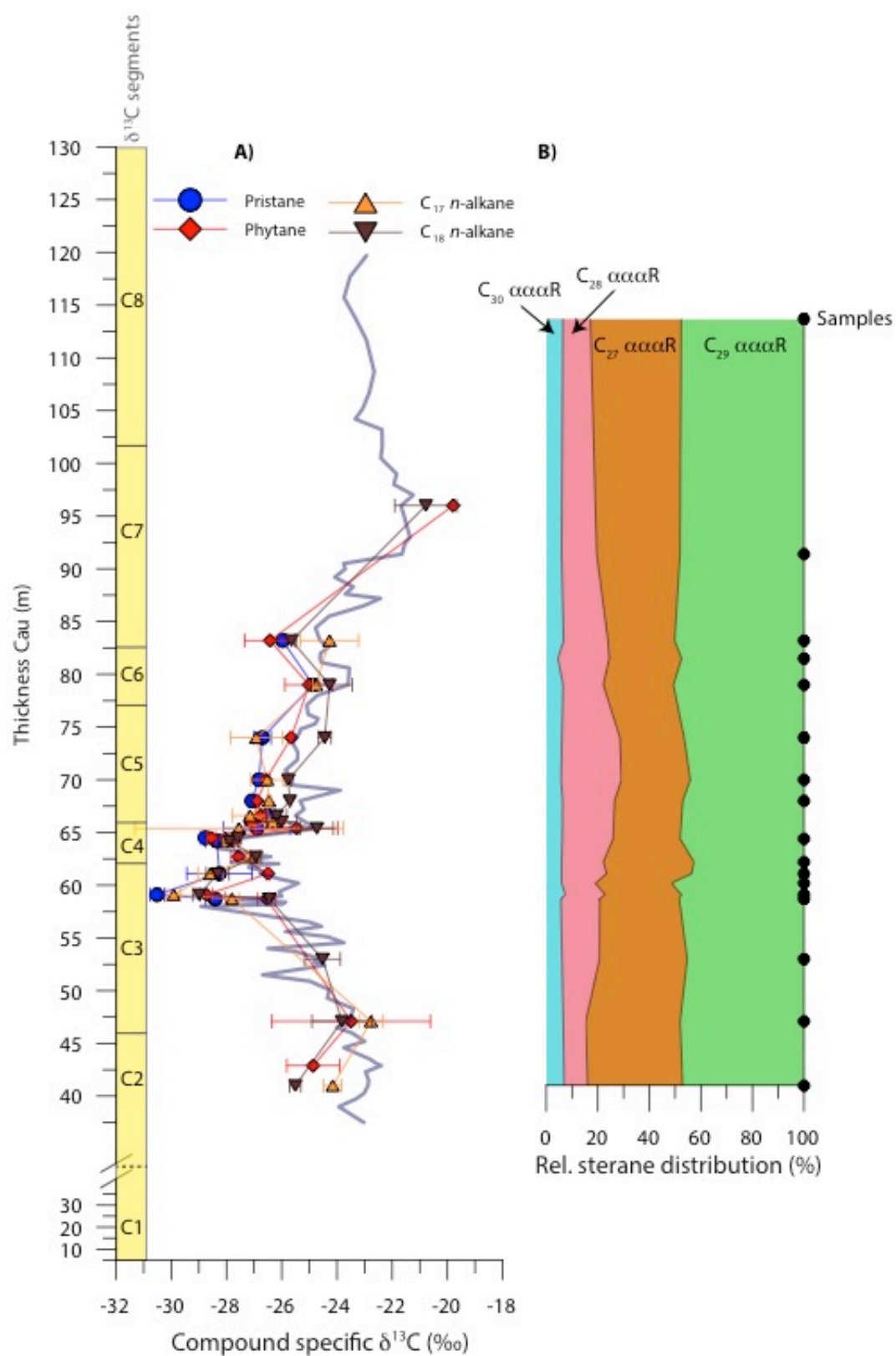


**Figure S3: Sterane distribution at Cau**

a)  $\delta^{13}\text{C}_{\text{TOC}}$  and  $\delta^{13}\text{C}_{\text{alg}}$  across OAE 1a at Cau together with b) relative  $\text{C}_{27}$ - $\text{C}_{30}$  αααR sterane distribution.



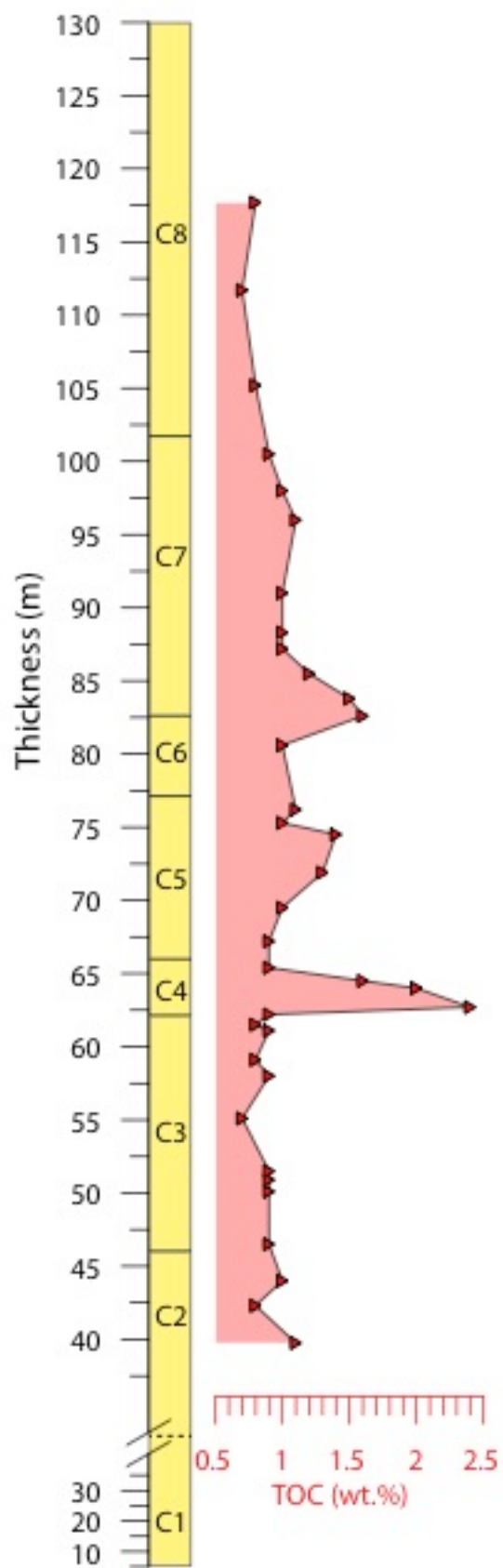
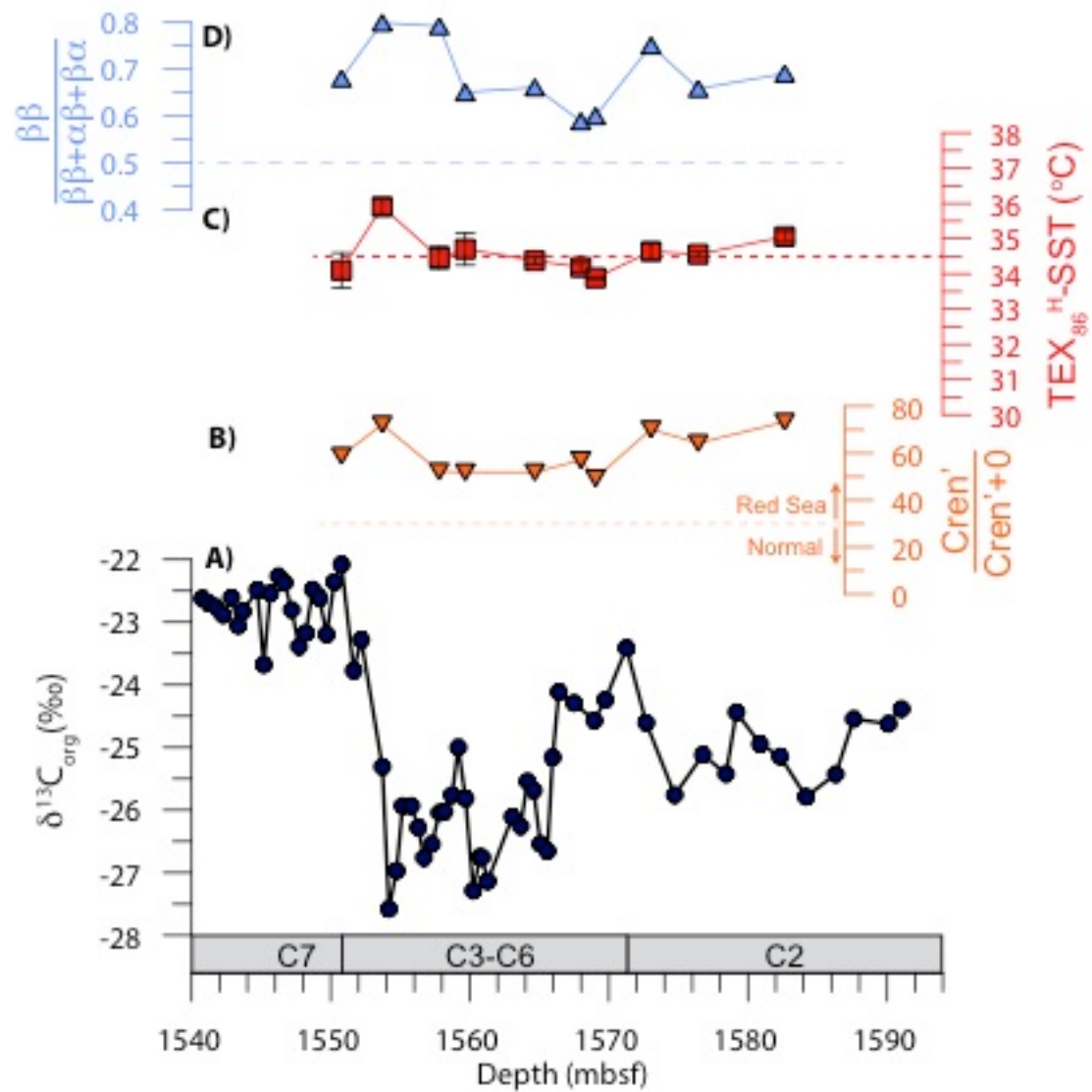
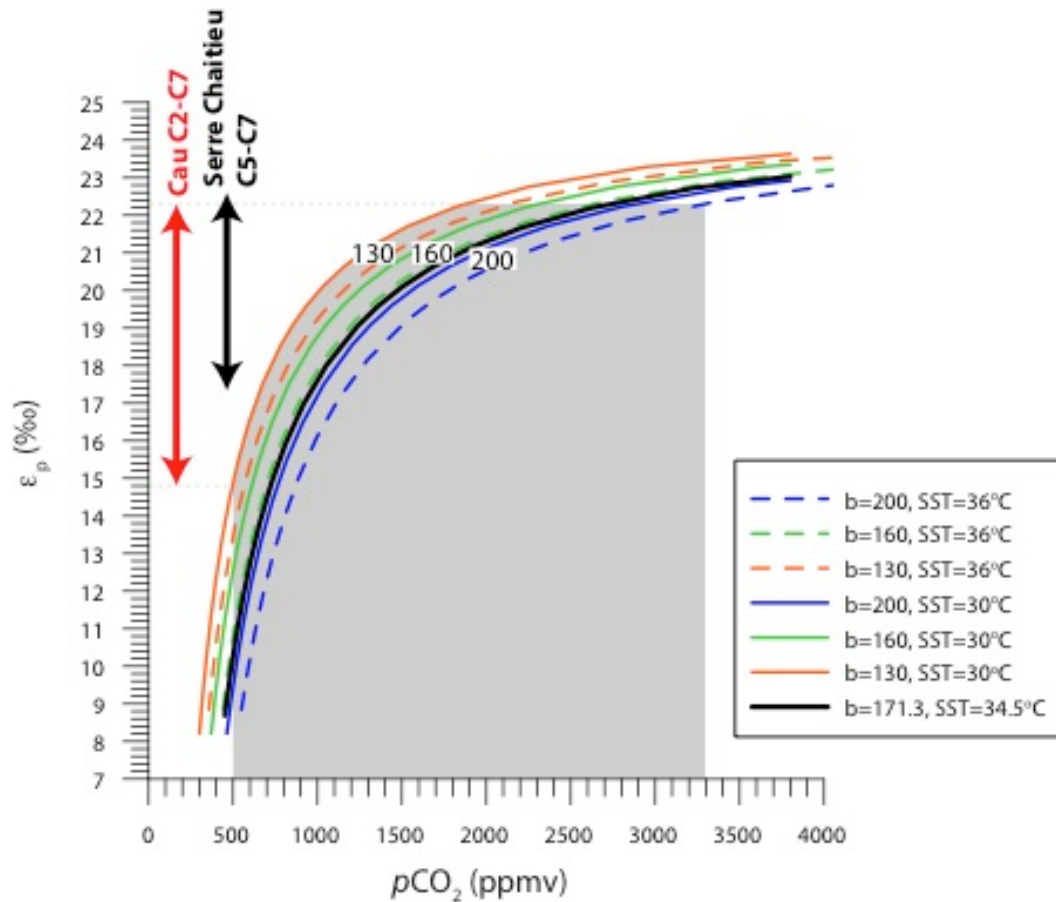


Figure S4; Total organic carbon (TOC) record from Cau.



**Figure S5; Sea surface temperatures across OAE 1a**

a) bulk  $\delta^{13}\text{C}_{\text{org}}$  across OAE 1a at DSDP Site 398 with C-isotope stratigraphy<sup>S2</sup> together with b) ratio of crenarchaeol abundance over GDGT-0, c) SSTs, based on the  $\text{TEX}_{86}^{\text{H}}$ -calibration<sup>S3</sup>, and d)  $\text{C}_{31}$  hopane maturity index. Error bars on  $\text{TEX}_{86}^{\text{H}}$ -SSTs represent  $1\sigma$  of duplicates.



**Figure S6; Relationship between  $\epsilon_p$  and  $p\text{CO}_2$**

The relationship between  $\epsilon_p$  and  $p\text{CO}_2$ , assuming SSTs values between 30 (continuous lines) and 36 °C (dashed lines) and  $b$  values of 130 (orange), 160 (green), and 200 (blue). For our  $p\text{CO}_2$  calculations we assumed a constant SST of 34.5 °C and  $b$  value of 171.3 (thick black line). The range of  $\epsilon_p$  values observed across segments C2 to C7 at Cau (red arrow) and segment C5 to C7 at Serre Chaitieu<sup>S4</sup> (black arrow) are also indicated.

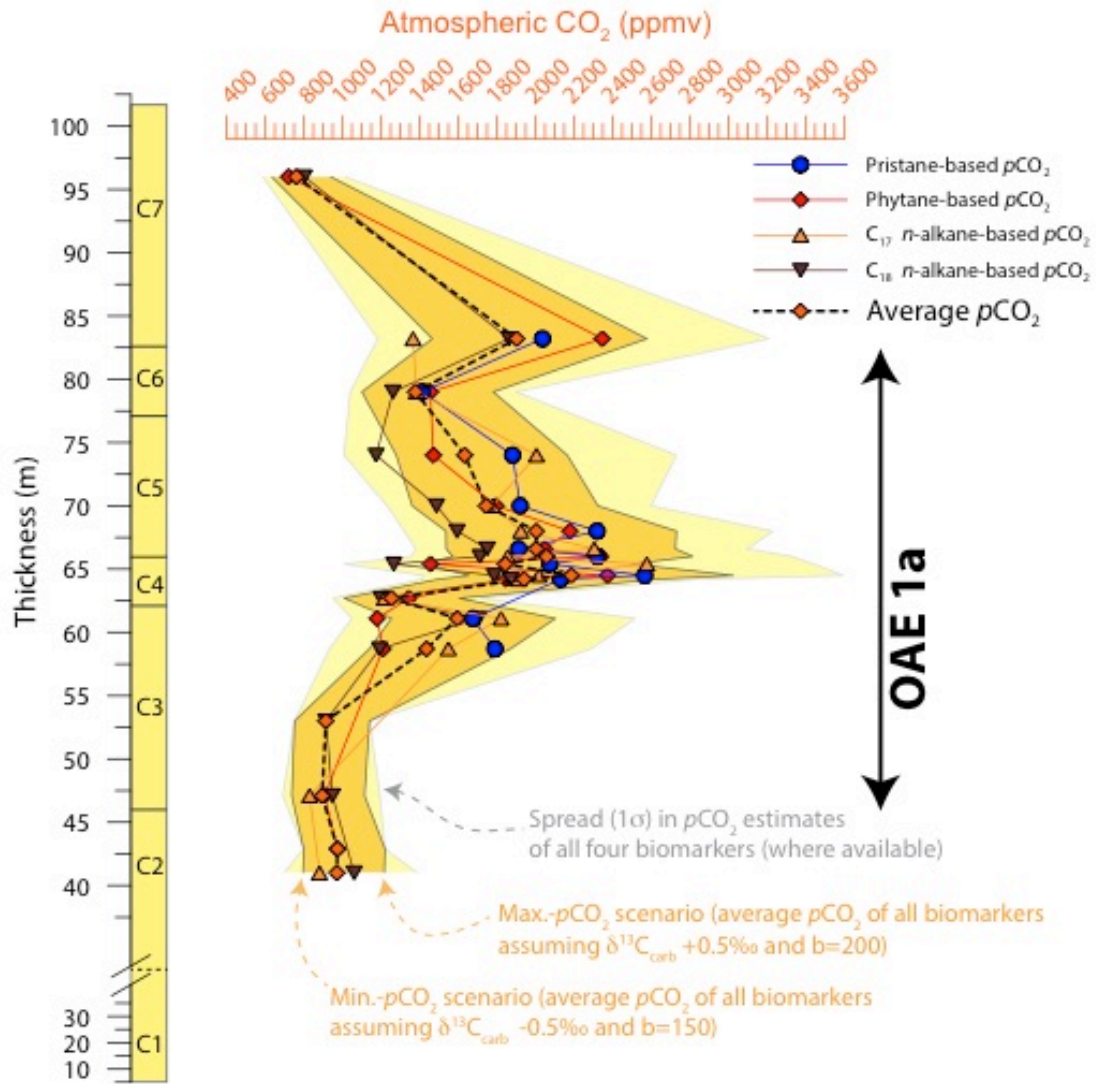


**Figure S7; Uncertainty envelopes**

$p\text{CO}_2$  estimates derived from the  $\delta^{13}\text{C}$  values of individual biomarkers, as well as the resulting average that is used in Figure 3 of the main manuscript.

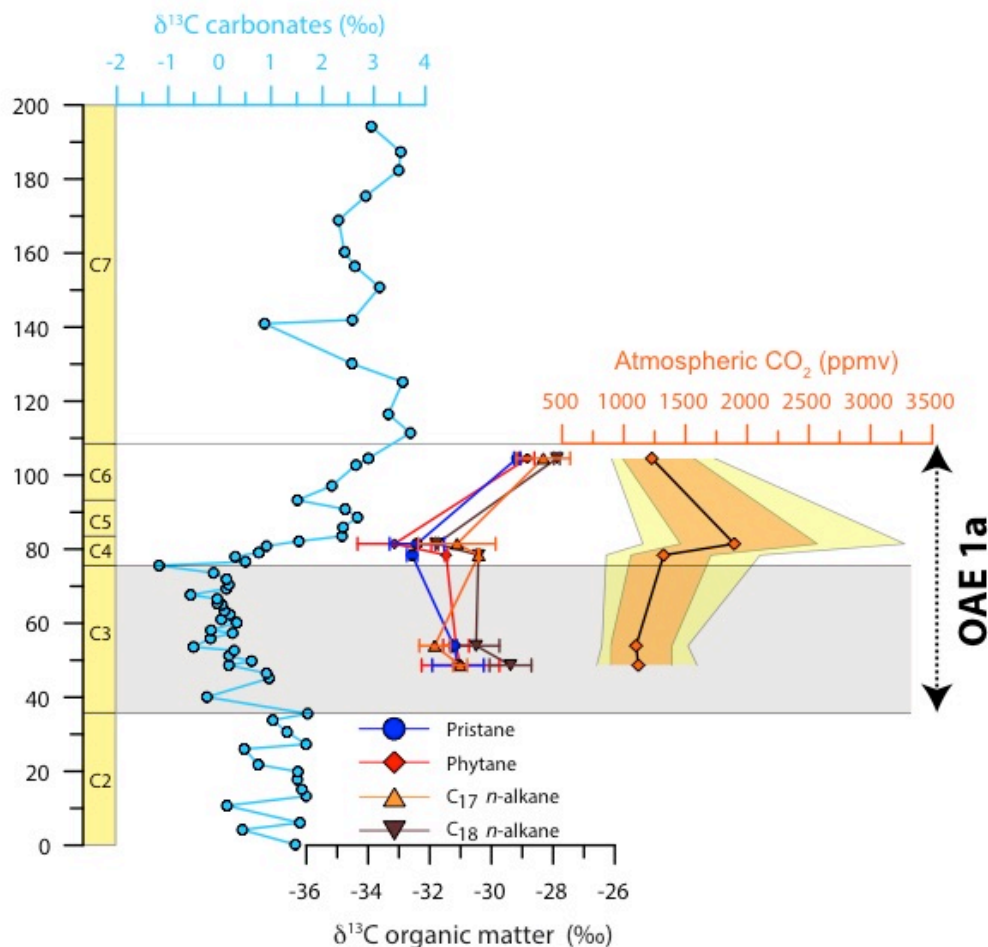


**Figure S8;  $\delta^{13}\text{C}$  and  $p\text{CO}_2$  Djebel Serdj formation in Tunisia**

$\delta^{13}\text{C}_{\text{carb}}^{\text{S5}}$  together with low-resolution  $\delta^{13}\text{C}_{\text{alg}}$  (not corrected to bulk biomass) and  $p\text{CO}_2$  record, calculated using the exact same assumption as used to calculate  $p\text{CO}_2$  at Cau.

#### Supplementary References

- S1 Kuhnt, W., Holbourn, A. & Moullade, M. Transient global cooling at the onset of early Aptian oceanic anoxic event (OAE) 1a. *Geology* **39**, 323-326 (2011).
- S2 Li, Y.-X. *et al.* Toward an orbital chronology for the early Aptian Oceanic Anoxic Event (OAE1a, ~ 120 Ma). *Earth Plant. Sc. Lett.* **271**, 88-100 (2008).
- S3 Kim, J.-H. *et al.* New indices and calibrations derived from the distribution of crenarchaeal isoprenoid tetraether lipids: Implications for past sea surface temperature reconstructions. *Geochim. Cosmochim. Ac.* **74**, 4639-4654 (2010).
- S4 Heimhofer, U., Hochuli, P. A., Herrle, J. O., Andersen, N. & Weissert, H. Absence of major vegetation and palaeoatmospheric  $p\text{CO}_2$  changes associated with oceanic anoxic event 1a (Early Aptian, SE France). *Earth Plant. Sc. Lett.* **223**, 303-318 (2004).
- S5 Heldt, M., Bachmann, M. & Lehmann, J. Microfacies, biostratigraphy, and geochemistry of the hemipelagic Barremian–Aptian in north-central Tunisia: Influence of the OAE 1a on the southern Tethys margin. *Palaeogeogr., Palaeoclimatol., Palaeoecol.* **261**, 246-260 (2008).